Fractional-Order Memory-Reset Hybrid Integrator-Gain System - Part I Frequency Domain Properties

Weise, C.; Wulff, K.; Hosseini, S. A.; Kaczmarek, M. B.; Hassan HosseinNia , S.; Reger, J.

DOI
10.1016/j.ifacol.2025.10.116

Publication date
2025

Document Version
Final published version

Published in
IFAC-PapersOnline

Available online at www.sciencedirect.com

ScienceDirect

IFAC Papers Online CONFERENCE PAPER ARCHIVE

IFAC PapersOnLine 59-16 (2025) 277–282

Fractional-Order Memory-Reset Hybrid Integrator-Gain System – Part I: Frequency Domain Properties

C. Weise * **K. Wulff** * **S. A. Hosseini** ** **M. B. Kaczmarek** **
S. H. HosseinNia ** **J. Reger** *,1

* *Control Engineering Group, Technische Universität Ilmenau, P.O. Box 10 05 65, D-98684, Ilmenau, Germany*
** *Department of Precision and Microsystems Engineering, Delft University of Technology, Delft, The Netherlands*

Abstract: We introduce a fractional-order generalization of the hybrid integrator-gain system (HIGS) with memory reset of the fractional-order operator when re-enter the integration mode. We compute the describing function for rational orders in terms of Mittag-Leffler functions. The concepts also allow for the evaluation of the higher-order harmonics. For the implementation we represent higher-order approximations by combining first-order reset elements with an integrator. The fractional-order extension without memory reset can also be approximated using the same framework. Finally we show how the approximation affects the describing function.

1. INTRODUCTION

The hybrid integrator-gain system (HIGS) limits the output of an integrator such that it is sector bounded with respect to the input (Deenen et al., 2017). Hence it combines two linear elements: a pure integrator and a gain. Although only two linear elements are connected, the HIGS overcomes some limitations of pure linear control. For the frequency domain analysis, the frequency response of the HIGS is approximated by its describing function. As it only switches between integration and pure amplification of the input signal, its describing function does not depend on the input amplitude and can be interpreted as a nonlinear frequency response showing an amplitude response similar to a first-order system whereas the phase only drops to $-38°$ for high frequencies. In combination with linear filters the HIGS allows the construction of amplitude responses with a constant slope of -20db/decade while the phase response shows a lead for higher frequencies. Using the HIGS for loop-shaping yields larger phase margin and bandwidth, increasing the robustness significantly (Heertjes et al., 2023). These advantages together with the accessibility of this nonlinear approach in the frequency domain proved valuable in several engineering applications, like precision motion control (Deenen et al., 2017; Heertjes et al., 2017, 2023) and active vibration isolation (Sharif, 2023).

The works by Van den Eijnden et al. (2018) and Van Eijk et al. (2023) show how the HIGS can be combined with linear filters to exploit its properties and design nonlinear bandpass and lag filters. A second generalization leads towards fractional-order integration. It is introduced in Hosseini et al. (2022) where the order of integration provides an additional tuning parameter for loop shaping. The benefit of a lower order of integration leads to a reduced phase drop in the describing function for high frequencies. In comparison to integer-order (IO) derivatives fractional-order (FO) differential operators introduce a non-local memory, i.e. an FO derivative of a function at any given time-instant depends on the complete time-history before and not only on a limited (infinitesimal short) time interval. Our approach includes the reset of this memory in addition to hybrid dynamics. As the element is only included in the controller the memory is accessible and can be reset. The corresponding describing function still shows an advantageous lower phase drop compared to the IO-HIGS without the required ideally charged memory.

The remainder of this contribution is structured as follows. In Section 2 the definitions of the applied FO operators are given. Furthermore the describing functions for the IO-HIGS and its FO extension are discussed. The following section introduces a generalization of the HIGS element towards FO integration. Unlike the FO-HIGS considered in Hosseini et al. (2022) the memory of the fractional operator is reset when re-entering the integration mode. This simplifies the hybrid element as only two sectors are required and we can derive the describing function without the assumption of a perfectly charged memory. We apply a higher-order IO approximation of the FO integral to implement both hybrid FO elements to emphasize the differences between both approaches. Finally, Section 4 gives a simulation example before conclusions are drawn.

2. PRELIMINARY RESULTS AND DEFINITIONS

This section revisits the definition of the IO- and FO-HIGS and their frequency domain properties.

2.1 Fractional-Order Operators and LTI Systems

Non-integer order derivatives combine classical IO derivatives with the FO integral. By Podlubny (1999) we have

$$ {}_{t_0}\mathcal{I}^{\alpha} f(t) = \frac{1}{\Gamma(\alpha)} \int_{t_0}^{t} (t-\tau)^{\alpha-1} f(\tau) \mathrm{d}\tau, \quad t > t_0, \tag{1} $$

[1] Corresponding author: johann.reger@tu-ilmenau.de

10.1016/j.ifacol.2025.10.116

with the order of integration $\alpha \in \mathbb{R}^+$ and Euler's Gamma function $\Gamma(\cdot)$. The order of concatenation of the FO integral and the IO derivative result in different definitions of the FO derivative operator. Here we use Caputo's operator (Podlubny, 1999; Monje et al., 2010)

$$ {}_0\mathcal{D}_t^\alpha f(t) = \frac{1}{\Gamma(m-\alpha)} \int_{t_0}^{t} \frac{f^{(m)}(t)}{(t-\tau)^{\alpha-m+1}} \mathrm{d}\tau, \qquad (2) $$

where $\alpha \in \mathbb{R}^+$ is the differentiation order and m is an integer such that $m-1 \leq \alpha < m$. Due to the FO integral contained in this operator, the FO derivative is non-local as it acts with respect to the time limits t_0 and t.

The FO-LTI system with (classical) initialization reads:

$$ \Sigma_{\mathrm{FO}}: \begin{cases} {}_0\mathcal{D}^\alpha x(t) = Ax(t) + Bu(t), \quad x(0) = x_0 & \text{(3a)} \\ y(t) = Cx(t) + Du(t) & \text{(3b)} \end{cases} $$

with (pseudo) state $x(t) \in \mathbb{R}^n$, input $u(t) \in \mathbb{R}^p$, output $y(t) \in \mathbb{R}^q$, order of differentiation $\alpha \in (0, 2]$ and matrices A, B, C and D of appropriate dimensions.

The Mittag-Leffler function solves the initial value problem (Podlubny, 1999; Monje et al., 2010)

$$ x(t) = \mathcal{E}_{\alpha,1}(At^\alpha)x_0 + \int_0^t \tau^{\alpha-1}\mathcal{E}_{\alpha,\alpha}(A\tau^\alpha)Bu(t-\tau)\mathrm{d}\tau, \quad (4) $$

with $$ \mathcal{E}_{\alpha,\beta}(z) = \textstyle\sum_{k=0}^{\infty} \frac{z^k}{\Gamma(\alpha k+\beta)}, \qquad \alpha, \beta > 0. \quad (5) $$

2.2 Integer- and Fractional-Order HIGS

The IO-HIGS is given by Deenen et al. (2017, 2021); Heertjes et al. (2017) and takes the form

$$ \mathcal{H}_{\mathrm{IO}}: \begin{cases} \dot{x}(t) = \omega_h e(t), & (e, \dot{e}, u) \in \mathcal{F}_{\mathrm{IO},1} \quad \text{(I-Mode)} & \text{(6a)} \\ x(t) = k_h e(t), & (e, \dot{e}, u) \in \mathcal{F}_{\mathrm{IO},2} \quad \text{(P-Mode)} & \text{(6b)} \\ u(t) = x(t) & & \text{(6c)} \end{cases} $$

with $k_h > 0$ and $\omega_h > 0$ and the sector bound defined by

$$ \mathcal{F}_{\mathrm{IO},1} = \left\{ (e, \dot{e}, u) \in \mathbb{R}^3 | eu \geq \tfrac{1}{k_h} u^2 \wedge (e, \dot{e}, u) \notin \mathcal{F}_{\mathrm{IO},2} \right\} $$
$$ \mathcal{F}_{\mathrm{IO},2} = \left\{ (e, \dot{e}, u) \in \mathbb{R}^3 | u = k_h e \wedge \omega_h e^2 > k_h e\dot{e} \right\}. $$

Its describing function (Van den Eijnden et al., 2018) is shown in Fig. 1 for $\omega_h = 1$ and $k_h = 1$. The amplitude response corresponds to a first-order system low-pass filter with stationary gain k_h and a corner frequency of $\omega_c = \left|1 + 4\mathrm{j}\pi^{-1}\right| \omega_h k_h^{-1}$. The phase response however shows only a phase drop of 38° which may improve the robustness-margins of the control system. As the HIGS element produces a continuous output the higher order harmonics (see Van Eijk et al. (2023) for details) are not dominant in comparison to non-smooth reset control.

A first generalization of the HIGS towards FO integration gives (Hosseini et al., 2022)

$$ \mathcal{H}_{\mathrm{FO}}: \begin{cases} {}_0\mathcal{D}^\alpha x(t) = \omega_h e(t), & (e, \dot{e}, u) \in \mathcal{F}_1 & \text{(7a)} \\ x(t) = k_h e(t), & (e, \dot{e}, u) \in \mathcal{F}_2 & \text{(7b)} \\ x(t) = 0, & (e, \dot{e}, u) \in \mathcal{F}_3 & \text{(7c)} \\ u(t) = x(t) & & \text{(7d)} \end{cases} $$

with $k_h > 0, \omega_h > 0$, $\alpha \in (0, 1)$ and the sectors defined by

$$ \mathcal{F} = \left\{ (e, \dot{e}, u) \in \mathbb{R}^3 | eu \geq \tfrac{1}{k_h} u^2 \right\} \quad \mathcal{F}_1 = \mathcal{F} \backslash (\mathcal{F}_2 \cup \mathcal{F}_3) $$
$$ \mathcal{F}_2 = \{ (e, \dot{e}, u) \in \mathcal{F} | u = k_h e \wedge (\omega_h e \; {}_0\mathcal{D}_t^\alpha e > k_h \dot{e} e \vee $$
$$ e \; {}_0\mathcal{D}_t^\alpha e < 0 \vee \left(e = 0 \wedge \omega_h \dot{e} \; {}_0\mathcal{D}_t^{1-\alpha} e > k_h \dot{e}^2 \right) \} $$
$$ \mathcal{F}_3 = \left\{ (e, \dot{e}, u) \in \mathcal{F} | u = 0 \wedge \omega_h e^2 > k_h e\dot{e} \right\}. $$

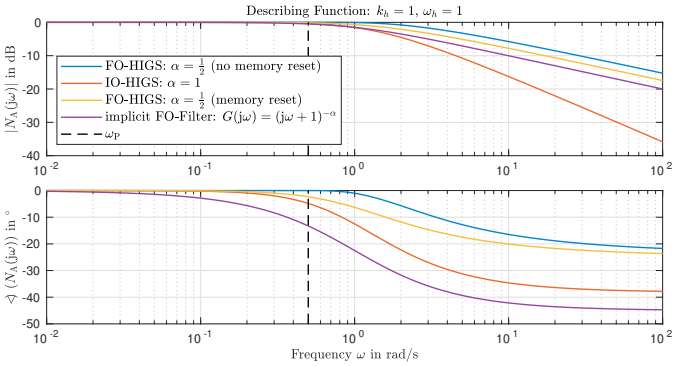

Fig. 1. Describing function of different hybrid elements.

As in the IO case the element contains the (fractional-order) integration (7a) (I-mode) in the domain $\mathcal{F}_1$ and the pure gain mode (7b) (P-Mode) in $\mathcal{F}_2$. Compared to the IO-HIGS this element requires an additional region $\mathcal{F}_3$ as the non-local memory of the operator allows the trajectories $(e(t), u(t))$ to leave the sector at the lower sector bound $(u = 0)$. This happens for negatively charged memory while the output is restricted to the gain mode.

As the FO operator builds up memory the describing function analysis for this element is based on the assumption that the memory is charged accordingly as the time tends to infinity. For $\gamma = \omega t \in [0, \pi]$ the output of the FO-HIGS with nonzero memory is approximated by

$$ u(\gamma) = \begin{cases} \frac{\omega_h}{\omega^\alpha} \left(\sin\left(\gamma - \alpha\frac{\pi}{2}\right) + \sin\left(\alpha\frac{\pi}{2}\right) \right), & \gamma \in [0, \gamma^*) \\ k_h \sin(\gamma), & \gamma \in [\gamma^*, \pi]. \end{cases} $$

With $s_\alpha = \sin(\alpha\pi/2)$ and $c_\alpha = \cos(\alpha\pi/2)$ the intersection results in $\gamma^* = \max\left(0; 2\arctan\left((\omega^\alpha k_h - \omega_h c_\alpha/(\omega_h s_\alpha)\right)\right)$. For low frequencies the initial derivative of the output $\dot{u}(0)$ exceeds $k_h\omega$ leading to a negative intersection time. Therefore γ^* is restricted to be positive, leading to a pure P-mode for $\omega < \omega_P = (c_\alpha\ \omega_h/k_h)^{1/\alpha}$. With the coefficients

$$ a_1 = \tfrac{\omega_h}{\omega^{\alpha+1}} \left(\tfrac{c_\alpha}{2} \sin^2(\gamma^*) - \tfrac{s_\alpha}{2}\gamma^* - s_\alpha \sin(\gamma^*) \right) - \tfrac{k_h}{2\omega} \sin^2(\gamma^*) $$
$$ b_1 = \tfrac{\omega_h c_\alpha}{\omega^{\alpha+1}} \left(\tfrac{\gamma^*}{2} - \tfrac{\sin(2\gamma^*)}{4} \right) + \tfrac{k_h}{2\omega} \left[\pi - \gamma^* \right] - $$
$$ \tfrac{\omega_h s_\alpha}{\omega^{\alpha+1}} \left(\tfrac{\sin^2(\gamma^*)}{2} + \cos(\gamma^*) - 1 \right) + \tfrac{k_h \sin(2\gamma^*)}{4\omega} $$

the describing function reads $\mathcal{N}_{\mathrm{FO}}(\mathrm{j}\omega) = b_1(\omega) + \mathrm{j}a_1(\omega)$.

Fig. 1 shows the Bode-plot of this describing function for $k_h = \omega_h = 1$ and the integration order $\alpha = \frac{1}{2}$. For frequencies lower than ω_P the element shows a pure gain mode. For high frequencies we see a slope of -20α dB/decade and a reduced phase drop compared to the IO-HIGS. However, the phase drop does not scale linearly with α. The higher order harmonics are given by Hosseini et al. (2024).

3. FO-HIGS WITH MEMORY RESET

The new approach avoids the definition of a third region by resetting the memory to zero when the trajectory enters the gain mode

$$ \tilde{\mathcal{H}}_{\mathrm{FO}}: \begin{cases} {}_{t_k}\mathcal{D}_t^\alpha x(t) = \omega_h e(t), & (e, \dot{e}, u) \in \tilde{\mathcal{F}}_1 & \text{(8a)} \\ x(t) = k_h e(t), & (e, \dot{e}, u) \in \tilde{\mathcal{F}}_2 & \text{(8b)} \\ u(t) = x(t) & & \text{(8c)} \end{cases} $$

with $k_h > 0$, $\omega_h > 0$, the order of integration $\alpha \in (0, 1)$ and the memory reset instances t_k defined by

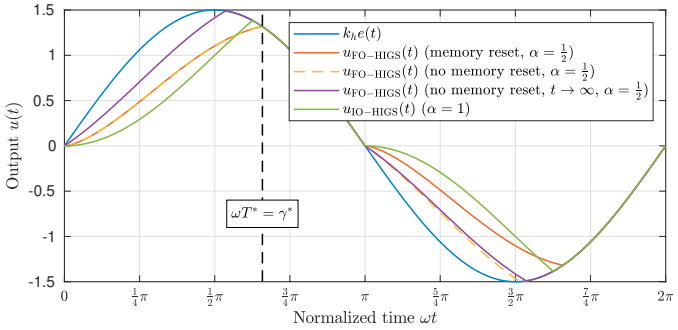

Fig. 2. Time-response to a sinusoidal input of the different hybrid integrators.

$$\left(e(t_k^-),\dot{e}(t_k^-),u(t_k^-)\right)\in\tilde{\mathcal{F}}_2 \qquad \left(e(t_k^+),\dot{e}(t_k^+),u(t_k^+)\right)\in\tilde{\mathcal{F}}_1$$

and $t_0=0$ and $k\in\mathbb{N}_0$. The sector bounds are given by

$$\tilde{\mathcal{F}}_1=\left\{(e,\dot{e},u)\in\mathbb{R}^3 | eu\geq\tfrac{1}{k_h}u^2\wedge(e,\dot{e},u)\notin\tilde{\mathcal{F}}_2\right\}$$
$$\tilde{\mathcal{F}}_2=\left\{(e,\dot{e},u)\in\mathbb{R}^3 | u=k_he\wedge\omega_he^2>k_he\,({}_{t_k}\mathcal{D}_t^{\alpha}e(t))\right\}.$$

As the memory is reset once the trajectories re-enter the I-mode ($\tilde{\mathcal{F}}_2$), no negative memory can build up and the output u cannot leave the sector at the lower bound ($u\equiv 0$).

3.1 Describing-Function and Higher-Order Harmonics

Similar to the IO-HIGS we derive the describing function of the FO memory reset HIGS to enable the tuning in the frequency domain. We consider the sinusoidal input $e(t)=\sin(\omega t)$ and approximate the output $u(t)$ with its Fourier series expansion with coefficients for $\kappa=1,2,\ldots$

$$\bar{a}_\kappa=\frac{\omega}{\pi}\int_0^{2\pi/\omega}u(t)\cos(\kappa\omega t)\mathrm{d}t,\ \bar{b}_\kappa=\frac{\omega}{\pi}\int_0^{2\pi/\omega}u(t)\sin(\kappa\omega t)\mathrm{d}t. \quad (9)$$

This yields the describing function $\tilde{\mathcal{N}}_{\mathrm{FO}}(\mathrm{j}\omega)=\bar{b}_1+\mathrm{j}\bar{a}_1$.

The output of the FO-HIGS (7a) for $\alpha=\frac{1}{2}$ is shown in Fig. 2 in comparison to the other HIGS elements. As in the IO case (green) the output is symmetrical in each half period (red), i.e. for $\omega t\in[\pi,\pi+\gamma^*]$ the output u is negative of the initialization interval $\omega t\in[0,\gamma^*]$. In the FO case without memory reset (dashed yellow line) we only see this if the memory is charged perfectly (purple line).

For $\omega t\in[0,\pi]$ the output of the FO-HIGS with memory reset (zero memory) is given by:

$$u(t)=\begin{cases}\dfrac{\omega_h}{\Gamma(\alpha)}\displaystyle\int_0^t(t-\tau)^{\alpha-1}\sin(\omega\tau)\mathrm{d}\tau, & \omega t\in[0,\gamma^*)\\ k_h\sin(\omega t), & \omega t\in[\gamma^*,\pi]\,.\end{cases} \quad (10)$$

Compared to the nonzero memory case the output trajectories show a zero derivative at the initial time as

$$\lim_{t\to0}\tfrac{\mathrm{d}}{\mathrm{d}t}\left({}_0\mathcal{I}^{\alpha}\omega_h\sin(\omega t)\right)=\lim_{s\to\infty}s^2\left(\tfrac{\omega_h}{s^{\alpha}}\tfrac{\omega}{s^2+\omega^2}\right)=0.$$

For this reason the memory reset FO-HIGS does not show a pure gain mode at low frequencies.

For an analytic expression of the FO integral of the sinusoidal input, we resort to rational orders $\alpha\in\mathbb{Q}$, such that we can incorporate IO models in a higher dimensional (pseudo) state-space. We rewrite the sinusoidal input as the output of an IO generator system:

$$\dot{x}_s=\begin{pmatrix}0&-\omega\\ \omega&0\end{pmatrix}x_s=A_sx_s,\qquad x_s(0)=\begin{pmatrix}0\\-1\end{pmatrix} \quad (11a)$$
$$y_s=\begin{pmatrix}1&0\end{pmatrix}x_s=C_sx_s=\sin(\omega t). \quad (11b)$$

For rational orders $\alpha=p/q$ with $p,q\in\mathbb{N}$ we represent the generator system by an associated FO system as in (Weise et al., 2017) with $\underline{\alpha}=1/q$ and $\bar{x}_s^\top(0)=(x_s^\top(0)\ \ 0)^\top$:

$$\mathcal{D}^{\underline{\alpha}}\bar{x}_s=\begin{pmatrix}0&I_{2(q-1)\times2(q-1)}\\ A_s&0\end{pmatrix}\bar{x}_s=\bar{A}_s\bar{x}_s,$$
$$y_s=\begin{pmatrix}C_s&0_{1\times2(q-1)}\end{pmatrix}\bar{x}_s=\bar{C}_s\bar{x}_s.$$

To derive the FO integral of the harmonic we add p FO integrators of the commensurate order $\underline{\alpha}$ resulting in

$$\mathcal{D}^{\underline{\alpha}}\begin{pmatrix}\tilde{x}\\ \bar{x}_s\end{pmatrix}=\begin{pmatrix}N_{p\times p}&e_p\bar{C}_s\\ 0&\bar{A}_s\end{pmatrix}\begin{pmatrix}\tilde{x}\\ \bar{x}_s\end{pmatrix}=A_{\sin}x_{\sin}$$

with the ith unit vector $e_i\in\mathbb{R}^{p\times1}$,

$$N_{p\times p}=\begin{pmatrix}0&I_{(p-1)\times(p-1)}\\ 0&0\end{pmatrix},\ e_p=(0\cdots0\ \ 1)^\top,$$

and $x_{\sin}(0)=(\tilde{x}^\top(0)\ \ \bar{x}_s^\top(0))^\top$. As the initial conditions vanish $\tilde{x}(0)=0$ the combined p derivatives of order $\underline{\alpha}$ result in the required order α although the additivity of FO derivative order does not hold in general. Hence the output is given by

$$u=\omega_h\begin{pmatrix}e_1^\top&0_{1\times2q}\end{pmatrix}x_{\sin}=C_{\sin}x_{\sin},$$

where e_1 is the first unit vector of length p. Finally the FO integral of the harmonic can be written in terms of matrix Mittag-Leffler functions:

$$u(t)=C_{\sin}\mathcal{E}_{\underline{\alpha},1}(A_{\sin}t^{\underline{\alpha}})x_{\sin}(0),\quad t\in[0,T^*].$$

At the time-instant T^* we finally have

$$u(t)=C_{\sin}\mathcal{E}_{\underline{\alpha},1}(A_{\sin}T^{*\underline{\alpha}})x_{\sin}(0)=k_h\sin(\omega T^*). \quad (12)$$

In contrast to the previous hybrid elements, the switching instant T^* has to be determined numerically in general. However, Eq. (12) allows a direct computation compared to the integration of the weakly singular term in (10), which is highly susceptible to the sampling time.

We split the integral to determine the Fourier coefficient

$$b_\kappa=\frac{2\omega}{\pi}\underbrace{\int_0^{T^*}u(t)\sin(\kappa\omega t)\mathrm{d}t}_{B_{\kappa,1}}+\frac{2\omega}{\pi}\underbrace{\int_{T^*}^{\pi/\omega}u(t)\sin(\kappa\omega t)\mathrm{d}t}_{B_{\kappa,2}}. \quad (13)$$

We can reshape the multiplication in the integral $B_{\kappa,1}$ to a suitable convolution with $\varphi=-\kappa\omega T^*$ leading to

$$B_{\kappa,1}=\int_0^{T^*}u(\tau)\sin(\kappa\omega\tau)\mathrm{d}\tau=-\int_0^{T^*}\sin\left(\kappa\omega(T^*-\tau)+\varphi\right)u(\tau)\mathrm{d}\tau.$$

Hence u can be interpreted as the input to the IO generator system with zero initial conditions ($\eta(0)=0$), i.e.

$$\dot{\eta}=\begin{pmatrix}0&-\kappa\omega\\ \kappa\omega&0\end{pmatrix}\eta+\begin{pmatrix}\sin(\kappa\omega T^*)\\ \cos(\kappa\omega T^*)\end{pmatrix}u=A_{\kappa\omega}\eta+B_{\kappa\omega}u \quad (14)$$

such that the terms $A_{\kappa,1}$ and $B_{\kappa,1}$ are given by

$$\begin{pmatrix}B_{\kappa,1}\\ A_{\kappa,1}\end{pmatrix}=-\begin{pmatrix}1&0\\0&1\end{pmatrix}\int_0^{T^*}\exp\left(A_{\kappa\omega}(T^*-\tau)\right)B_{\kappa\omega}u(\tau)\mathrm{d}\tau.$$

Rewriting the generator system in an FO representation allows the incorporation of the FO signal part (12) by an extended system with $\bar{B}_{\kappa\omega}^\top=\begin{pmatrix}0&B_{\kappa\omega}^\top\end{pmatrix}$:

$$\mathcal{D}^{\underline{\alpha}}\begin{pmatrix}\bar{\eta}\\ x_{\sin}\end{pmatrix}=\begin{pmatrix}\bar{A}_{\kappa\omega}&\bar{B}_{\kappa\omega}C_{\sin}\\ 0&A_{\sin}\end{pmatrix}\begin{pmatrix}\bar{\eta}\\ x_{\sin}\end{pmatrix},\ \begin{pmatrix}B_{\kappa,1}\\ A_{\kappa,1}\end{pmatrix}=(I\ 0\ 0)\begin{pmatrix}\bar{\eta}\\ x_{\sin}\end{pmatrix}$$

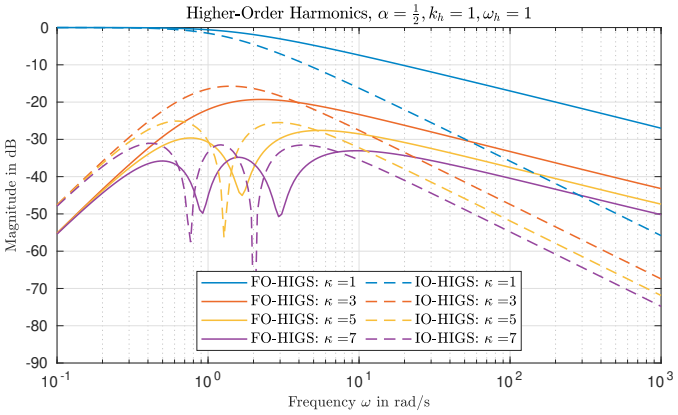

Fig. 3. Magnitude characteristics of the memory-reset FO-HIGS in comparison to the IO-HIGS.

with $\bar{A}_{e,\kappa} = \begin{pmatrix} \bar{A}_{\kappa\omega} & \bar{B}_{\kappa\omega} C_{\sin} \\ 0 & A_{\sin} \end{pmatrix}, \bar{A}_{\kappa\omega} = \begin{pmatrix} 0 & I_{2(q-1)\times 2(q-1)} \\ A_{\kappa\omega} & 0 \end{pmatrix}$. Finally the FO parts of the Fourier coefficients $A_{\kappa,1}$ and $B_{\kappa,1}$ can be expressed in terms of Mittag-Leffler functions, once the intersection time T^* is determined numerically

$$\begin{pmatrix} B_{1,\kappa} \\ A_{1,\kappa} \end{pmatrix} = (I\ 0\ 0)\, \mathcal{E}_{\underline{\alpha},1}\left(\bar{A}_{e,\kappa}(T^*)^{\underline{\alpha}}\right) \begin{pmatrix} \bar{\eta}(0) \\ x_{\sin}(0) \end{pmatrix}. \tag{15}$$

The remaining terms $A_{\kappa,2}$, $B_{\kappa,2}$ can be solved analytically as $u(t) = k_h \sin(\omega t)$. Due to the symmetry all even coefficients vanish. Giving us for the 1st-order harmonic ($\kappa = 1$)

$$B_{2,1} = \frac{k_h}{2}\left[\frac{\pi-\gamma^*}{\omega} + \frac{\sin(2\gamma^*)}{2\omega}\right], A_{2,1} = -\frac{k_h}{2\omega}\sin^2(\gamma^*). \tag{16}$$

with $\gamma^* = \omega T^*$, and for odd $\kappa \geq 3$ we have

$$B_{2,\kappa} = \frac{k_h}{2\omega}\left(-\frac{\sin((\kappa-1)\gamma^*)}{\kappa-1} + \frac{\sin((\kappa+1)\gamma^*)}{\kappa+1}\right) \tag{17}$$

$$A_{2,\kappa} = \frac{k_h}{2\omega}\left(\frac{\cos((1-\kappa)\gamma^*)}{1-\kappa} + \frac{\cos((1+\kappa)\gamma^*)}{(1+n)} + \frac{2}{\kappa^2-1}\right). \tag{18}$$

The describing function of the new element is depicted in Fig. 1 for the order of integration $\alpha = \frac{1}{2}$. For large frequencies it shows the expected slope of -10 dB/decade and also a lower phase drop compared to the IO-HIGS. In contrast to the describing function of the FO-HIGS without memory reset, it does not show a pure gain mode at low frequencies, and the corner frequency is lower.

The magnitude of the higher-order harmonics is shown in Fig. 3. As in the IO case the higher-order harmonics are not dominant in comparison to the describing function. In the FO element the maximum is reduced by about 3 dB as the FO integration of order $\alpha = \frac{1}{2}$ is closer to the gain mode as a pure integration.

3.2 Approximations and Generalized Hybrid Integrators

As FO operators contain infinite memory their implementation requires high order IO systems. It is common to use higher-order band-limited approximations, e.g. continuous fraction approximation (Monje et al., 2010) or the (refined) Oustaloup filter (Monje et al., 2010; Tepljakov et al., 2011), which is designed to mimic the FO operator for $\alpha \in (0,1)$ within a certain frequency range $\omega \in [\omega_{\text{low}}, \omega_{\text{high}}]$ obeying

$$s^\alpha \approx H_\alpha(s) = \omega_{\text{high}}^\alpha \prod_{k=-R}^{R} \frac{s+\omega_k^-}{s+\omega_k^+} \tag{19}$$

with $\omega_k^\pm = \omega_{\text{low}}\left(\omega_{\text{high}}/\omega_{\text{low}}\right)^{\frac{k+R+(1\pm\alpha)/2}{2R+1}}$, $R \in \mathbb{N}$. (20)

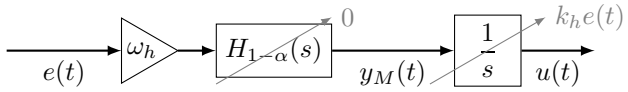

Fig. 4. Block diagram of the separated FO integration (21).

Any approximation of an FO integrator has to be adjusted to preserve the integration properties of the FO integrator for low frequencies. This can be achieved by splitting off an IO integrator as applied in HosseinNia (2013), i.e.

$$s^{-\alpha} = \frac{1}{s}s^{1-\alpha} \approx \frac{1}{s}H_{1-\alpha}(s). \tag{21}$$

The modes of $H_{1-\alpha}(s)$ represent the memory of the FO operator, while the continuous output is guaranteed by the subsequent integration (see Fig. 4). Overall this approach results in an approximation of order $N = 2R+2$.

By construction the transfer function $H_{1-\alpha}(s)$ only contains stable real poles and minimum-phase transfer zeros. The state-space realization of $H_{1-\alpha}(s)$ reads

$$\begin{aligned} \dot{z}_M(t) &= A_z z_M(t) + B_z \omega_h e(t) \\ y_M(t) &= C_z z_M(t) + D_z \omega_h e(t), \end{aligned}$$

which yields the overall approximation of the FO integral

$$\dot{z}_M(t) = A_z z_M(t) + B_z\, \omega_h e(t) \tag{22a}$$

$$\dot{z}_I(t) = C_z z_M(t) + D_z\, \omega_h e(t) \tag{22b}$$

$$\mathcal{I}^\alpha\left(\omega_h e(t)\right) \approx u(t) = z_I(t). \tag{22c}$$

With (22) the FO-HIGS with memory reset can be implemented as follows:

$$\tilde{\mathcal{H}}_{\text{FO}} \begin{cases} \begin{pmatrix} \dot{z}_M(t) \\ \dot{z}_I(t) \end{pmatrix} = \begin{pmatrix} A_z z_M(t) + B_z \omega_h e(t) \\ C_z z_M(t) + D_z \omega_h e(t) \end{pmatrix}, & (e,\dot{e},u) \in \bar{\mathcal{F}}_1 \\ \qquad \text{(I-mode)} \\ \begin{pmatrix} z_M(t) \\ z_I(t) \end{pmatrix} = \begin{pmatrix} 0 \\ k_h e(t) \end{pmatrix}, & (e,\dot{e},u) \in \bar{\mathcal{F}}_2 \\ \qquad \text{(P-mode)} \\ u(t) = z_I(t), \end{cases}$$

with $\bar{\mathcal{F}}_1 = \mathcal{F} \backslash \bar{\mathcal{F}}_2$ and

$$\bar{\mathcal{F}}_2 = \left\{(e,\dot{e},u) \in \mathbb{R}^3 | u = k_h e \wedge (C_z z_M + D_z \omega_h e) e > k_h e \dot{e}\right\}.$$

The memory states z_M are set to zero when the element is in the gain-mode, i.e. $(e,\dot{e},u) \in \bar{\mathcal{F}}_2$. Therefore the IO approximation $\tilde{\mathcal{H}}_{\text{FO}}$ combines $N-1$ first-order reset elements with an integrator. As the reset condition is given in terms of the in- and output of the element however, it does not show the same behavior as a series connection of first-order reset elements and an IO-HIGS. The reset to zero is also a key element in the passivity and stability analysis in Weise et al. (2025).

In comparison to that, the memory remains unchanged in the element presented in (Hosseini et al., 2022)

$$\hat{\mathcal{H}}_{\text{FO}} \begin{cases} \dot{z}_M(t) = A_z z_M(t) + B_z \omega_h e(t), & (e,\dot{e},u,z_M) \in \mathbb{R}^{2+N} \\ \dot{z}_I(t) = C_z z_M(t) + D_z \omega_h e(t), & (e,\dot{e},u,z_M) \in \hat{\mathcal{F}}_1 \\ z_I(t) = k_h e(t), & (e,\dot{e},u,z_M) \in \hat{\mathcal{F}}_2 \\ z_I(t) = 0, & (e,\dot{e},u,z_M) \in \hat{\mathcal{F}}_3 \\ u(t) = z_I(t) \end{cases}$$

with the adjusted sector defined by $\hat{\mathcal{F}}_1 = \mathcal{F} \backslash (\hat{\mathcal{F}}_2 \cup \hat{\mathcal{F}}_3)$ and

$$\hat{\mathcal{F}}_2 = \left\{(e,\dot{e},u,z_M) \in \mathbb{R}^q | u = k_h e \wedge \beta(z_M,e) e > k_h e \dot{e}\right\},$$

$$\hat{\mathcal{F}}_3 = \left\{(e,\dot{e},u,z_M) \in \mathbb{R}^q | u = 0 \wedge e \neq 0 \wedge \beta(z_M,e) e < 0\right\},$$

where $\beta(z_M,e) = (C_z A_z z_M + D_z \omega_h e)$ and $q = N+2$.

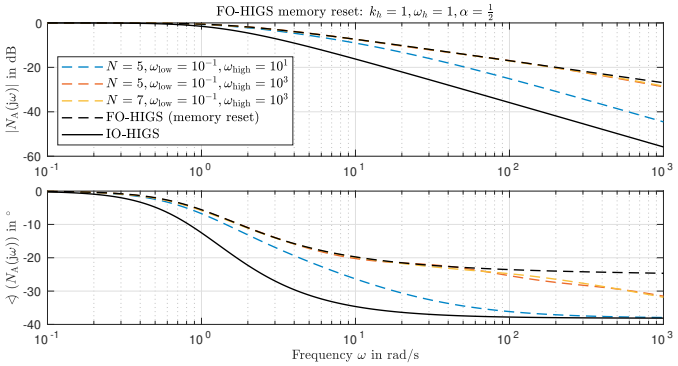

Fig. 5. Frequency response for different approximation orders N of the FO-HIGS with memory reset.

The input e influences the memory state z_M at any time and this state affects the switching conditions. In the P-mode ($\hat{\mathcal{F}}_2$) and 0-mode ($\hat{\mathcal{F}}_3$) the state z_M is not visible at the output u of the element. The describing function of the approximations can be computed using similar steps as in Section 3.1 without the need of the FO expansion. For a sinusoidal input the output of (22) reads

$$u(t) = \begin{cases} \bar{C}_z \int_0^t e^{\left(\bar{A}_z (t-\tau)^{\alpha-1}\right)} \bar{B}_z \sin(\omega\tau) \mathrm{d}\tau, & t \in [0, \bar{T}^*) \\ k_h \sin(\omega t), & t \in \left[\bar{T}^*, \frac{\pi}{\omega}\right] \end{cases}$$

with $\bar{A}_z = \begin{pmatrix} A_z & 0 \\ C_z & 0 \end{pmatrix}$, $\bar{B}_z = \omega_h \begin{pmatrix} B_z \\ D_z \end{pmatrix}$, $\bar{C}_z = (0 \cdots 1)$.

Once more we make use of the generator system (11) to express the convolution in terms of a matrix exponential

$$u(t) = \bar{C}_{\sin} \exp\left(\bar{A}_{\sin} t\right) \bar{x}_{\sin}(0), \quad t \in [0, \bar{T}^*]$$

with $\bar{A}_{\sin} = \begin{pmatrix} \bar{A}_z & \bar{B}_z C_\omega \\ 0 & A_s \end{pmatrix}$, $\bar{C}_{\sin} = \begin{pmatrix} \bar{C}_z^\top \\ 0 \end{pmatrix}^\top$, $\bar{x}_{\sin}(0) = \begin{pmatrix} 0 \\ x_s(0) \end{pmatrix}$.

Despite the simplification $\bar{T}^*$ is transcendentally given by

$$\bar{C}_{\sin} \exp\left(\bar{A}_{\sin} \bar{T}^*\right) \bar{x}_{\sin}(0) = k_h \sin(\omega \bar{T}^*).$$

Finally the Fourier coefficients are computed analogously as in the FO case and the first part reads

$$\begin{pmatrix} \bar{B}_{1,\kappa} \\ \bar{A}_{1,\kappa} \end{pmatrix} = (I \ 0) \exp\left(\begin{pmatrix} A_\omega & B_\omega \bar{C}_{\sin} \\ 0 & \bar{A}_{\sin} \end{pmatrix} \bar{T}^* \right) \begin{pmatrix} 0 \\ \bar{z}_{\sin}(0) \end{pmatrix}.$$

Eqs. (16),(17) give the second part changing T^* to $\bar{T}^*$.

Fig. 5 shows the frequency responses for the different approximations of the FO-HIGS with memory reset. The lower frequency range is dominated by the proportional mode, hence ω_{low} can be chosen just below the corner frequency. The upper approximation bandwidth ω_{high} should be chosen faster than the desired bandwidth of the element. For higher frequencies the describing function tends towards the IO-HIGS, which is most evident if ω_{high} is chosen relatively low (compare Fig. 5 blue dashed line). Increasing ω_{high} leads to the desired frequency response within a desired frequency range while the required number of states N is relatively small. Note that the computation of the describing function of the approximation is not restricted to rational orders α.

The approximation also allows to compute the describing function in case the memory is not reset. By assumption the memory is perfectly charged by the sinusoidal input, i.e. $y_M(t) = \beta_\omega \sin(\omega t + \varphi_\omega)$ with $\beta_\omega = |H_{1-\alpha}(\mathrm{j}\omega)|$ and $\varphi_\omega = \arg\left(H_{1-\alpha}(\mathrm{j}\omega)\right)$. This results in the output

$$u(t) = \begin{cases} \frac{\omega_h \beta_\omega}{\omega} \left[\cos(\varphi_\omega) - \cos(\omega t + \varphi_\omega)\right], & \omega t \in [0, \bar{\gamma}] \\ k_h \sin(\omega t), & \omega t \in [\bar{\gamma}, \pi]. \end{cases}$$

This allows for an analytic solution of the intersection $\bar{\gamma}$

$$\bar{\gamma} = \max\left(0, 2 \arctan\left(\frac{k_h \omega}{\omega_h \beta_\omega \cos(\varphi_\omega)} - \tan(\varphi_\omega)\right)\right).$$

As the initial slope might exceed the pure gain mode, this also leads to a pure P-Mode for frequencies below $\bar{\omega}_{\text{P}}$ with $\omega_h \operatorname{Im}(H_{\alpha-1}(\mathrm{j}\bar{\omega}_{\text{P}})) = k_h \bar{\omega}_{\text{P}}$. The coefficients for the describing function are given by:

$$\begin{aligned} a_1 =& \frac{\omega_h \beta_\omega}{2\pi\,\omega} \Big[4\cos(\varphi_\omega)\sin(\bar{\gamma}) + \sin(\varphi_\omega) - \sin(2\bar{\gamma} + \varphi_\omega) - \\ & 2\bar{\gamma}\cos(\varphi_\omega) \Big] - \frac{k_h}{\pi} \sin^2(\bar{\gamma}) \\ b_1 =& \frac{\omega_h \beta_\omega}{2\pi\,\omega} \Big[3\cos(\varphi_\omega) + \cos(2\bar{\gamma} + \varphi_\omega) + 2\bar{\gamma}\sin(\varphi_\omega) - \\ & 4\cos(\bar{\gamma})\cos(\varphi_\omega) \Big] + \frac{k_h}{2\pi} \big[2(\pi - \bar{\gamma}) + \sin(2\bar{\gamma}) \big]. \end{aligned}$$

The derivation of the corresponding higher-order harmonics follows directly from the evaluation of (9). The approximation effects are similar to the case with memory reset. The upper approximation bandwidth ω_{high} has to be chosen faster than the desired bandwidth of the element to generate the desired phase response. For too small ω_{high} the approximation tends towards an IO-HIGS element for high frequencies. The approximation order N can be chosen relatively small.

4. SIMULATION EXAMPLE

In this section we use the proposed FO-HIGS to construct HIGS-based integrators using both IO and FO-HIGS. We compare their transient and steady-state performances in closed loop to that of a linear integrator.

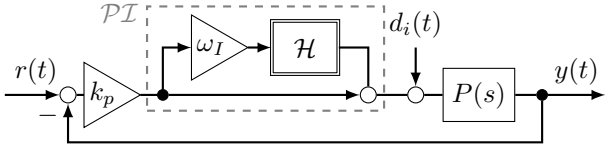

Fig. 6. Block diagram of the closed loop system.

Consider the first-order plant $P(s) = 1/(s+10)$ controlled by a proportional-integral (PI) element, as depicted in Fig. 6. Two nonlinear integrators with

$$C_1(s) = \left(1 + \frac{s}{\omega_r}\right)^\alpha \quad \text{and} \quad C_2(s) = \frac{1}{s}, \ \omega_r \in \mathbb{R}^+ \tag{24}$$

replace the integration part (see Fig. 7) . The nonlinear PI controllers are tuned to achieve a bandwidth of 10 Hz with parameters given in Tab. 1. The order $\alpha = 0.65$ is chosen to illustrate the effect of the fractional order (i.e. $\alpha \not\approx 1$) and provide the desired phase margin (i.e. $\alpha > 0.3$). The two nonlinear controllers exhibit nearly the same magnitude as the linear PI controller but differ in their phase characteristics. Note that the non-proper filter C_1 is implemented using $C_1'(s) = C_1(s)\,(1 + s/\omega_f)^{-1}$ with sufficiently large $\omega_f \in \mathbb{R}^+ \gg 1$.

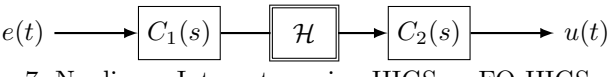

Fig. 7. Nonlinear Integrator using HIGS or FO-HIGS.

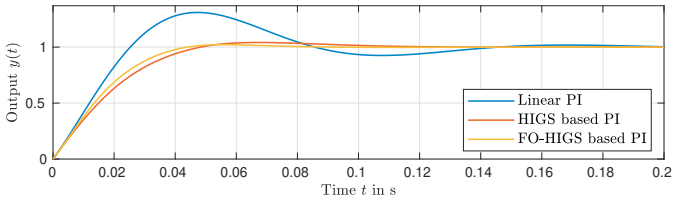

Fig. 8. Step response of the closed-loop system.

Tab. 1. Controller parameter and performance.

Name	k_h	ω_h	ω_r	ω_i	k_p	Overshoot	RMSE
PI (Linear)	-	-	-	88	37.05	30.9%	1
PI ($\alpha=1$)	1	46.5	12	88	37.05	4.1%	1.031
PI ($\alpha=0.65$)	1	6.7	5	88	37.05	2.2%	1.012

The step responses of the three closed loops are depicted in Fig. 8. We observe that the two control loops with nonlinear controllers show remarkably less overshoot with similar rise-time. This significant improvement in the transient response can be attributed to the additional phase introduced by their nonlinear nature. A slight improvement is also observed for the FO-HIGS compared to the IO-HIGS-based PI, which may be due to the fact that it provides more phase in its linear base system.

Tab. 1 also gives the overshoot of the step responses for the closed loops with the three designed controllers, along with the normalized steady-state root-mean-square error (RMSE) resulting from an input disturbance $d_i(t) = 0.01\sin(100\pi t)$. The controllers exhibit nearly identical steady-state error performance. This shows that the transient response has been significantly improved maintaining steady-state performance.

In our design the nonlinear controllers exhibit only a 15° phase advantage over the linear controller. It is worth noting that, using a HIGS-based controller, it is possible to achieve up to a 52° phase advantage. However, such an approach would compromise the reliability of the describing function and degrade steady-state performance due to the influence of higher-order harmonics. Even in the current scenario, where the HIGS element remains fully nonlinear at high frequencies, a small difference in the RMS value is observed compared to the FO controller.

5. CONCLUSIONS

We propose and analyze a fractional-order generalization of the HIGS with memory reset of the fractional-order operator. The reset of the memory simplifies the FO-HIGS element compared to previously considered FO-HIGS elements without reset. As the possibly negative memory is deleted when re-entering the integration mode, the trajectories $(e(t), u(t))$ cannot leave the sector at the lower limit $(u = 0)$, hence the 0-mode is not required and only the gain and integration mode are present. We derive a method to efficiently compute the describing function of the element and to analyze higher-order harmonics. Compared to the classical HIGS the FO versions provide a lower phase drop for higher frequencies leading to larger phase margins. These properties remain in the approximation of the FO operators within the desired frequency range. Through higher-order approximations, we can proof the passivity of the proposed element, see Weise et al. (2025). These approximations combine first-order reset elements with an IO-HIGS, therefore the results are not limited to the original FO integration.

REFERENCES

Deenen, D., Heertjes, M., Heemels, W., and Nijmeijer, H. (2017). Hybrid integrator design for enhanced tracking in motion control. In *American Control Conference*, 2863–2868.

Deenen, D.A., Sharif, B., van den Eijnden, S., Nijmeijer, H., Heemels, M., and Heertjes, M. (2021). Projection-based integrators for improved motion control: Formalization, well-posedness and stability of hybrid integrator-gain systems. *Automatica*, 133, 109830.

Heertjes, M., Eijnden, S.V.D., and Sharif, B. (2023). An Overview on Hybrid Integrator-Gain Systems with applications to Wafer Scanners. In *IEEE International Conference on Mechatronics*, 1–8.

Heertjes, M., Irigoyen, N., and Deenen, D. (2017). Data-driven tuning of a hybrid integrator-gain system. In *IFAC World Congress*, 10851–10856.

Hosseini, S.A., Tavazoei, M.S., Van Eijk, L.F., and HosseinNia, S.H. (2022). Generalizing Hybrid Integrator-Gain Systems Using Fractional Calculus. In *IEEE Conference on Control Technology and Applications*, 1050–1055.

Hosseini, S.A., van Eijk, L.F., Kaczmarek, M.B., and HosseinNia, S.H. (2024). Higher-order sinusoidal-input describing function analysis of fractional-order hybrid integrator-gain systems. *IFAC Conference on Advances in Proportional-Integral-Derivate Control*, 400–405.

HosseinNia, S.H. (2013). *Fractional Hybrid Control Systems: Modeling, Analysis and Applications to Mobile Robotics and Mechatronics*. Ph.D. thesis, Universidad de Extremadura, Spain.

Monje, C., Chen, Y., Vinagre, B., Xue, D., and Feliu, V. (2010). *Fractional-Order Systems and Controls: Fundamentals and Applications*. Springer.

Podlubny, I. (1999). *Fractional Differential Equations*. Acad. Press.

Sharif, B. (2023). *Formalization, Analysis, and Sampled-Data Design of Hybrid Integrator-Gain Systems*. Ph.D. thesis, Eindhoven University of Technology.

Tepljakov, A., Petlenkov, E., and Belikov, J. (2011). Fomcon: Fractional-order modeling and control toolbox for matlab. In *18th International Conference on Mixed Design of Integrated Circuits and Systems*, 684–689.

Van den Eijnden, S., Knops, Y., and Heertjes, M. (2018). A Hybrid Integrator-Gain Based Low-Pass Filter for Nonlinear Motion Control. In *IEEE Conference on Control Technology and Applications*, 1108–1113.

Van Eijk, L.F., Beer, S., Van Es, R.M.J., Kostić, D., and Nijmeijer, H. (2023). Frequency-Domain Properties of the Hybrid Integrator-Gain System and Its Application as a Nonlinear Lag Filter. *IEEE Transactions on Control Systems Technology*, 31(2), 905–912.

Weise, C., Wulff, K., Hosseini, S.A., Kaczmarek, M.B., HosseinNia, S.H., and Reger, J. (2025). Fractional-Order Memory-Reset Hybrid Integrator-Gain System - Part II: Stability Analysis. In *IFAC Symposium on Robust Control Design*.

Weise, C., Wulff, K., and Reger, J. (2017). Fractional-Order Observer for Integer-Order LTI Systems. In *Asian Control Conference*, 2101–2106.